Experimental Neurology 311 (2019) 293–304

Contents lists available at ScienceDirect

Experimental Neurology

journal homepage: www.elsevier.com/locate/yexnr

Research paper

Neuronal and vascular deficits following chronic adaptation to high altitude

Nathan P. Cramer[a,b], Alexandru Korotcov[b,c], Asamoah Bosomtwi[b,c], Xiufen Xu[a,b], Derek R. Holman[a,d], Kathleen Whiting[a,e], Scott Jones[b,c], Andrew Hoy[b,c], Bernard J. Dardzinski[b,c], Zygmunt Galdzicki[a,b,d,e,*]

[a] Department of Anatomy, Physiology and Genetics, F. Edward Hébert School of Medicine, Uniformed Services University of the Health Sciences, Bethesda, MD, United States
[b] Center for Neuroscience and Regenerative Medicine, F. Edward Hébert School of Medicine, Uniformed Services University of the Health Sciences, Bethesda, MD, United States
[c] Department of Radiology and Radiological Sciences, F. Edward Hébert School of Medicine, Uniformed Services University of the Health Sciences, Bethesda, MD, United States
[d] Molecular & Cell Biology Graduate Program, F. Edward Hébert School of Medicine, Uniformed Services University of the Health Sciences, MD, United States
[e] Neuroscience Graduate Program, F. Edward Hébert School of Medicine, Uniformed Services University of the Health Sciences, Bethesda, MD, United States

ARTICLE INFO

Keywords:
Hypobaric-hypoxia
Memory
MRI
Angiogenesis
Neuroinflammation
Corpus callosum
Action potential conductance
RNA-Seq
Real-time PCR
Fear-conditioning
Novel-object recognition
Cxcl12//SDF1

ABSTRACT

We sought to understand the mechanisms underlying cognitive deficits that are reported to affect non-native subjects following their prolonged stay and/or work at high altitude (HA). We found that mice exposed to a simulated environment of 5000 m exhibit deficits in hippocampal learning and memory accompanied by abnormalities in brain MR imaging. Exposure (1–8 months) to HA led to an increase in brain ventricular volume, a reduction in relative cerebral blood flow and changes in diffusion tensor imaging (DTI) derived parameters within the hippocampus and corpus callosum. Furthermore, neuropathological examination revealed significant expansion of the neurovascular network, microglia activation and demyelination within the corpus callosum. Electrophysiological recordings from the corpus callosum indicated that axonal excitabilities are increased while refractory periods are longer despite a lack of change in action potential conduction velocities of both myelinated and unmyelinated fibers. Next generation RNA-sequencing identified alterations in hippocampal and amygdala transcriptome signaling pathways linked to angiogenesis, neuroinflammation and myelination. Our findings reveal that exposure to hypobaric-hypoxia triggers maladaptive responses inducing cognitive deficits and suggest potential mechanisms underlying the adverse impacts of staying or traveling at high altitude.

1. Introduction

Extended exposure to high altitude (HA) environments is associated with prolonged cognitive deficits (Abraini et al., 1998; Ryn, 1979, 1988; Subudhi et al., 2014). In the early phase of exposure, acute mountain sickness (AMS) and the more severe conditions of HA pulmonary or cerebral edema (HAPE/HACE) are well recognized and can be treated effectively with prescription medications (Leaf and Goldfarb, 2007; Netzer et al., 2013; Swenson, 2016). Long-term effects of HA exposure on overall physical and mental health can be more challenging to diagnose (Abraini et al., 1998; Cavaletti et al., 1990; León-Velarde et al., 2005; Regard et al., 1989; Sharma et al., 2014; Subudhi et al., 2014), but maladaptive physiological effects may have a significant role in altered cognitive performance in non-native subjects working, living in or relocating to HA (Chen et al., 2016; Fan and Kayser, 2016). Indeed, HA exposure frequently results in persistent neuropathological and behavioral deficits including spatial memory impairment (Nelson et al., 1990; Rimoldi et al., 2016; Shukitt-Hale et al., 1994; Virués-Ortega et al., 2004; Zhang et al., 2013) but the mechanisms linking the two phenomena remain unclear (Kauser et al., 2014; Prasad et al., 2013).

Magnetic resonance imaging (MRI) and electroencephalogram (EEG) studies in humans have provided key insights into potential mechanisms by noting alterations in brain structure and function of individuals following sojourns to HA (Chen et al., 2016; Hunt et al., 2013; Richardson et al., 2011; Yan et al., 2010, 2011). These adaptive or maladaptive functional responses can be linked to anatomical changes such as abnormalities within major white matter tracts (Kottke

* Corresponding author at: Uniformed Services University of the Health Sciences, F. Edward Hébert School of Medicine, Department of Anatomy, Physiology and Genetics, Bethesda, MD 20814, United States.
E-mail address: zgaldzicki@usuhs.edu (Z. Galdzicki).

https://doi.org/10.1016/j.expneurol.2018.10.007
Received 7 June 2018; Received in revised form 20 September 2018; Accepted 10 October 2018
Available online 13 October 2018

et al., 2015; Zhang et al., 2012) and reduced grey matter volume (Di Paola et al., 2008; Fayed et al., 2006; Foster et al., 2015). Additional white matter abnormalities and lower performance on cognitive tests have been reported in U-2 pilots who operated at cabin altitudes of approximately 29,000 ft (McGuire et al., 2013, 2014). Hemosiderin deposits, representative of microbleeds, are also frequently observed following exposure to HA (Kallenberg et al., 2008; Schommer et al., 2013) suggesting vascular disruption may contribute to HA pathology. Indeed, impaired cerebral autoregulation of blood supply was found in subjects living or transiently present at HA (Appenzeller et al., 2004; Jansen et al., 2000; Norcliffe et al., 2005). Furthermore, regional changes in cerebral blood flow (Feddersen et al., 2015) and arterial diameters (Imray et al., 2014) are linked to altered EEG. These adaptive mechanisms appear to be strongly influenced by genetic background (Claydon et al., 2008) and indicate that a comprehensive investigation of the effects of HA on neuropathology must examine this process from a structural, functional and genetic viewpoint.

In our previous study, we showed that exposure to HA causes time-dependent changes in mouse respiratory function and motor behavior consistent with adaptive changes in the nervous system (Cramer et al., 2015). Here we report that mice similarly exposed to HA exhibit hippocampal mediated memory deficits with accompanying abnormal MR imaging in the brain consistent with neurovascular changes, increased inflammation and white matter remodeling. Pathological and transcriptome analysis suggest that vascular remodeling and inflammation contribute to HA-induced cognitive deficits. Thus, the results reported here provide novel insights into functional mechanisms underlying time-dependent changes occurring in response to HA and highlight multiple potential targets for therapeutic interventions.

2. Materials and methods

2.1. Animals

All procedures were approved by the USUHS Institutional Animal Care and Use Committee and results are presented according to ARRIVE guidelines. Sample sizes for each experiment were based on previous experience and results from similarly applied techniques in published research. For behavioral experiments, male C57Bl6/J were obtained from Jackson Laboratories to arrive at the Uniformed Service University of the Health Sciences (USUHS) at 7 weeks of age and were housed on a reverse light cycle at sea level for one week prior to HA exposure. Environmental variables are as regulated by the Department of Laboratory Animal Medicine at USUHS and follow AAALAC guidelines. All mice were randomly assigned to experimental groups and were socially housed up to 5 mice per cage. Control mice, which resided at sea level (SL), were also housed on a reversed light cycle. Due to significant differences in body weights between HA and SL mice (Cramer et al., 2015), blinding was not possible for in vivo experiments. For immunohistochemistry and magnetic resonance imaging (MRI) male B6.129P-Cx3cr1tm1Litt/J mice (a transgenic line of mice on the C57Bl6/J background that express GFP in immune cells such as microglia) were obtained from breeding colonies maintained at USUHS using homozygous males obtained from Jackson Laboratories paired with standard C57Bl6/J females. As with the behavioral experiments, resulting male heterozygous CX3CR1-GFP mice entered the HA simulation chamber at 8 weeks of age. Immunohistochemical and MRI experiments used separate cohorts of mice as the mice that underwent in vivo imaging continued to progress in a separate study. Separate cohorts of mice were used for each MRI time point.

2.2. Simulated HA exposure

Mice were group housed in conventional cages inside a modified Vicker's hypobaric chamber altered by Reimers System Inc. (Lorton, VA) to operate under reduced pressures (~7.4 psi) using a vacuum pump (Welch Model 2585B or 2067B-01) as previously described (Cramer et al., 2015). Ascent to a simulated altitude of 5000 m (HA, equivalent to an inspired PO_2 of 78 mmHg) proceeded at 200 m per minute and return to SL proceeded at the same rate. Environmental parameters (pressure, oxygen and carbon dioxide levels, temperature and relative humidity) inside the chamber were continuously monitored using custom built sensors from CO2Meter Inc. (Ormond Beach, FL). The chamber was located within the common animal vivarium to ensure consistent environmental parameters across exposure groups and conditions. Mice in the sea level control groups were housed within the vivarium but not within the HA chamber. The chamber altitude was monitored using a data logging digital manometer (AZ Instrument Corp., Taichung City, Taiwan). Cage maintenance was performed at SL at least once per week. All mice were monitored daily for signs of distress such as social isolation, failure to groom or excessive weight loss.

2.3. Fear conditioning

C57Bl6/J mice were housed at either SL or HA ($n = 8$ per group) for 3-weeks prior to the onset of fear conditioning. This time point corresponds to a period of early stabilization in the adaptation process (Cramer et al., 2015). For the initial training session, mice were acclimated to the testing room for 5 min prior to being placed individually in Plexiglass chambers with a wire grid floor inside a dimly lit enclosure (Ugo Basile, Varese Italy). Black and white striped or checkered backdrop lining the walls of the enclosure were used to strengthen the context association. Mouse movements were recorded and analyzed for freezing behavior using ANY-maze software (Stoelting Co., Wood Dale, IL). The training session consisted of a two-minute acclimation period followed by five 0.5 mA foot shocks spaced 1 min apart. Mice were returned to their home cages (either at HA or SL) at the end of the test. Context dependent memory formation was tested by returning the mice to identical chambers at 24 h and 1, 3, 8 and 12-weeks after the training session. During these tests mice were monitored for freezing behavior and no additional foot shocks were delivered. Analysis was performed on the first 3 min of each session to coincide with the training session pre-shock period prior to the association of the environment with the aversive foot shock. Since the weight of HA mice were significantly different, as reported before, the investigator could be aware to which experimental group each mouse belonged (Cramer et al., 2015).

2.4. Novel object recognition

Our novel object recognition protocol was developed based on published procedures (Antunes and Biala, 2012). Briefly, after a 30 min room acclimation period, 3 month exposed mice and their respective controls ($n = 13$ each) were placed individually in open field containers (Stoelting Co., Wood Dale, IL) and allowed to explore their empty environment for an additional 30 min. These periods served to acclimate the mice both to the room and the containers in which the novel object recognition (NOR) test would take place. Approximately 30 min after the acclimation period, mice were returned to the open field containers in which two identical objects (either Duplo blocks or similarly sized plastic cylinders) were placed equidistant from the corners of the apparatus. Mice were allowed to explore both objects for 15 min after which they were returned to their home cage. One hour later the mice were returned to the open field containers in which new objects had been placed. One object was identical to the previously explored objects and the other was novel (Duplo block or cylinder). The type of novel object and its location was assigned randomly to avoid object or place preferences. No objects were reused within a test and each apparatus was thoroughly cleaned with 70% ethyl alcohol to minimize residual odor cues effect. A discrimination index was calculated using the equation: $DI = (T_{Novel} - T_{Familiar})/(T_{Novel} + T_{Familiar})$, where T_{Novel} and $T_{Familiar}$ are the times spent exploring the novel and familiar objects

respectively. The DI of one SL mouse was more than two standard deviations below the group mean and was eliminated from the data set.

2.5. MRI acquisition and measurements

All MRI experiments were conducted using a 7 T Bruker Biospec 70/20 USR Superconducting Magnet System (Bruker Biospin, Inc., Billerica, MA) with isoflurane anesthetized mice. Heart and respiratory rates and body temperature were continuously monitored (SA-instruments, Stony Brook, NY). Separate cohorts of CX3CR1-GFP mice were imaged after 1, 3.5, 6, and 8 months of HA exposure along with age matched controls. All mice underwent: anatomical proton density/T2 weighted (*PDW/T2W*) imaging for general assessment, structural changes, and edema formation; arterial spin labeling (*ASL*) to compute relative cerebral blood flow (r*CBF*) maps; Magnetic Resonance Angiography (*MRA*) for the direct visualization of the vascular structure; contrast enhanced MRA (CE-MRA) to calculate and analyze the vascular density index (VDi); and Diffusion Tensor Imaging (*DTI*) to estimate white matter (WM) integrity and reveal microstructural axonal damage. The brains of these mice were collected for follow-up 2-photon analysis with Scale-treatment rendering brain optically transparent (data not shown) (Hama et al., 2011). More specific details on scan parameters are provided in the Supplemental Methods.

2.6. Blood collection

As in our previous study (Cramer et al., 2015), whole blood samples were collected through cardiac puncture under isoflurane anesthesia or submandibular vein puncture using 5.5 mm Goldenrod Animal Lancets (MEDIpoint, Inc., Mineola NY). Samples were placed into EDTA-coated plastic tubes (BD, Franklin Lakes, New Jersey) and shipped for analysis to BioReliance Corp. (Rockville, MD) or Charles River Research Animal Diagnostic Services (Wilmington, MA) for complete blood count (CBC) with differential analysis.

2.7. Immunohistochemistry

Vasculature in 3-month HA-exposed ($n = 4$) and SL-control ($n = 5$) mice from cohorts separate from those used for MRI was labeled and fixed with 4% paraformaldehyde using the protocol developed by Robertson et al. (2014) and described in detail in the Supplementary Methods. Coronal brain sections were cut by Histoserv Inc. (Germantown, MD) and stored in the dark at −80 °C until imaging. Brain slices (10 μm thick) for microglia immunohistochemistry were generated in the same manner without tail vein injection. Luxol Fast Blue (LFB) colorimetric histological staining was performed on paired brains (1 HA and 1 SL in the same tissue block) cut and stained at the same time to ensure consistency of slice thickness and staining intensity. ROIs were similar to those used in MRI analysis. Endogenously expressed GFP in CX3CR1 heterozygous knock-in mice enabled visualization of microglia (Garcia et al., 2013) which were subsequently labeled with rabbit polyclonal anti-CD68 (Cat# ab125212, Lot GR238318–3; Abcam, Cambridge MA) diluted 1:200 and goat anti-rabbit IgG H&L (Alexa Fluor® 594) (AB150080; Abcam, Cambridge MA) diluted 1:100. Extravascular albumin was labeled with rabbit anti-mouse albumin (Cat# ab19196, Lot GR249722–16; Abcam, Cambridge MA) at 1:1000 to assess blood brain barrier integrity (Clasen et al., 1970; Saunders et al., 2015; Tischner et al., 2006). The sections were mounted with ProLong® Diamond Antifade Mountant with DAPI (P36971; ThermoFisher Scientific, Inc.). Images were acquired using a Leica AF6000 (Leica Microsystems Inc., Buffalo Grove, IL) or an Axio Scan.Z1 (Carl Zeiss Microscopy, LLC, Thornwood, NY). Images were analyzed using Arivis Vision4D imaging software (Arivis AG; Unterschleißheim, Germany) and ImageJ as described in the Supplementary Methods.

2.8. Electrophysiology

Mice ($n = 7$ HA and 8 SL) were anesthetized with isoflurane and the unperfused brains transferred to the cutting chamber of a Leica VT1200 vibratome containing chilled sucrose ACSF (in mM: sucrose 206, KCl 2, $CaCl_2$ 1, NaH_2PO_4 1.25, $MgSO_4$ 2, MgCl-6H_2O 2, $NaHCO_3$ 26, D-glucose 10, bubbled with a mixture of 95% O_2/5% CO_2). Coronal sections, 400 μm thick, were cut and transferred to normal ACSF (in mM: NaCl 126, KCl 3, $CaCl_2$ 2, NaH_2PO_4 1.25, $MgSO_4$ 2, $NaHCO_3$ 26, D-glucose 10, bubbled with a mixture of 95% O_2/5% CO_2) at 36 °C for 30 to 45 min followed by an additional recovery period of 1 h at room temperature. Recordings were performed in an immersion chamber in flowing normal ACSF at room temperature as previously described (Olmos-Serrano et al., 2016). All solutions were continuously bubbled with 95/5% O_2/CO_2. Analysis of compound action potential (CAP) velocities and amplitudes are described in the Supplementary Methods.

2.9. Transcriptome analysis

Mice exposed to HA and SL for 3 or 12-weeks (HA = 5 and SL = 5 at each time point) were perfused transcardially with nuclease free PBS and sacrificed by decapitation under isoflurane anesthesia. Brains were quickly dissected, frozen on dry ice and kept at −80 °C until the time of RNA isolation. Coronal brain sections were cut on a cryostat and hippocampi and amygdalae were micropunched using a 500 μm cannula under a microscope as previously described (Harashima et al., 2006a, 2006b). Total RNA was isolated from micropunched sections using the miRNeasy Mini Kit (Qiagen #217004, Germantown, MD), quantified by Qubit 2.0 Fluorometer 2.0 (ThermoFisher Scientific #Q32866, Waltham, MA) and quality was verified on Bioanalyzer 2100 (Agilent Technology at Hudson Alpha). Only samples containing > 100 ng with RIN > 8 were used for RNA-Seq performed by Hudson Alpha Institute of Biotechnology (Huntsville, AL). Paired-end sequencing with at least 25 million, 50–75 bp, paired-end reads was performed. The reads were aligned to mouse reference genome mm10/GRCm38 with Ensembl annotations using Bowtie2-RSEM with default options. Differential expression analysis was performed on estimated read counts from RSEM using DESeq2 with batch correction modeling (Anders et al., 2013; Love et al., 2014; Robinson et al., 2010). Aligned .bam files were sorted using Bamtools and converted to .tdf format for visualization using Integrative Genomics Viewer (IGV, Broad Institute, Cambridge, MA). Venn Diagrams were created using http://bioinformatics.psb.ugent.be/webtools/Venn/. Ontology pathway enrichment analysis was performed using Ingenuity Pathway Analysis (IPA, QIAGEN Bioinformatics, Redwood City, CA) for all transcripts fulfilling the criteria of p-adjusted < 0.1. Ontology bar plots and all volcano plots were generated using Microsoft Excel.

2.10. Quantitative real time RT-PCR

The same RNA samples used for RNA-Seq were also used to create cDNA for qPCR validation of transcript expression. RNA (1000 ng per sample) were retrotranscribed to cDNA with High-Capacity cDNA Reverse Transcription Kit (ThermoFisher Scientific, Waltham, MA USA #4368814). Real-time quantification of cDNA was performed with specific TaqMan gene expression assays (ThermoFisher Scientific, catalog #4331182; all amplicon lengths 50-150 bp) on an ABI 7900 real time PCR instrument (Applied Biosystems) and data were normalized to endogenous control β-actin (ActB: Mm02619580_g1). To determine transcript expression of C-X-C motif chemokine 12 (Cxcl12/SDF1: Mm00445553_m1), cDNA was diluted 1:2.5 and run according to the Taqman Gene Expression Master Mix protocol (ThermoFisher Scientific #4369016). To determine transcript expression of fms related tyrosine kinase 1 (Flt1: Mm00438980_m1), vitronectin (Vtn: Mm00495976_m1), fibronectin 1 (Fn1: Mm01256744_m1), and von Willebrand factor (Vwf: Mm00550376_m1), cDNA was diluted 1:5 before following the Taqman

Gene Expression Master Mix protocol. All samples were run in triplicate. Ct values were analyzed following guidelines of Applied Biosystems by the ΔΔCT method. Difference in expression between HA and SL conditions was evaluated by 2-tailed Student's *t*-test of mean ΔΔCT values, with statistical significance considered as *p*-value ≤.05.

2.11. Statistics and experimental design

Results of the fear conditioning tests were analyzed using two-way repeated measures ANOVAs with condition (SL or HA) and exposure time as the independent variables. When significant interactions were present ($p < .05$) post-hoc comparisons were performed using the Holm–Sidak method. Student's t-test was used for comparing means within a single time point (e.g. NOR) while a two-way ANOVA was used when including time as an independent variable. The presence of a significant difference between probability distribution curves was tested using the Kolmogorov–Smirnov test. Input-output relationships were examined by comparing the decay constants of nonlinear fits through the respective data sets. With the exception of transcriptome analysis as indicated above, an alpha of 0.05 in any test was taken to show a significant difference. All tests were performed in either SigmaPlot (Systat Software, Inc., San Jose, CA) or GraphPad Prism (GraphPad Software Inc., La Jolla, CA).

3. Results

3.1. HA exposure induces hippocampal mediated memory deficits

HA exposure has been associated with long lasting cognitive deficits (Abraini et al., 1998; Ryn, 1979, 1988; Subudhi et al., 2014). To understand the adaptive mechanisms underlying this phenomenon we tested mice exposed to chronic HA and corresponding SL controls in a hippocampus dependent fear conditioning paradigm. After a three-week acclimation period, mice were exposed to a context-dependent fear conditioning paradigm with re-exposure to the identical context at 24 h and 1, 3, 8 and 12-weeks after the initial training session. This timeline examines the acquisition and retention of the context associated memory shown to rely on hippocampal networks. There was a significant interaction between treatment and session ($p = .005$, $n = 8$ for all groups at each time point, two-way repeated measures ANOVA with Holm-Sidak post-hoc comparisons). Both HA and SL mice spent significantly more time freezing 24 h after the training session ($p = .001$ and $p < .001$ for HA and SL respectively). However, while the amount of freezing remained significantly elevated above the baseline training session levels in SL mice throughout the subsequent 12-weeks of testing, the degree of freezing returned to baseline levels in HA mice after only 1 week. In addition, HA mice spent significantly less time freezing compared to SL mice at all post-training time points (Fig. 1A; $p < .001$ at all-time points; Holm-Sidak post-hoc comparison). Similarly, in the novel object recognition test, which involves the lateral entorhinal cortex (Wilson et al., 2013), 3 month exposed HA mice showed significantly impaired object-context associations relative to their SL counterparts (Fig. 1B; $p = .021$, unpaired Student's *t*-test, $n = 12$ and 13; SL and HA per each group respectively).

3.2. MR imaging reveals structural and functional neurological changes

3.2.1. T2 values and ventricular volume

In order to examine the underlying neurological and vascular mechanisms of long-term adaptation to HA coincident with the decline in hippocampal mediated learning and memory we carried out neuroimaging using MRI after different time periods of HA exposure. As HA exposure can lead to edema we examined T2-weighted images (Fig. 2A) and T2 maps in a quantitative manner (Rumpel et al., 1995). The derived T2 values (Fig. 2B) were slightly elevated in the HA neocortex and hippocampus but these changes were not significant. However, in the corpus callosum (CC), T2 values were significantly elevated after 1 month of exposure and remained elevated relative to SL controls at the longer exposure time points.

As changes in anatomical brain structure have been reported in individuals who travel to HA (Di Paola et al., 2008; Fayed et al., 2006; Foster et al., 2015), we also examined the normalized ventricular volume (nVV) in HA mice relative to their SL controls (Fig. 2C). The nVV was increased in HA mice and, like the elevated T2 values, remained stable across the exposure time points.

To examine the abnormal T2 values in the CC more closely in vivo, we used diffusion tensor imaging (DTI) to estimate the integrity of white matter through measurement of apparent water diffusion coefficients and anisotropy (representative scans shown in Fig. 3A). Similar to our T2 results, we did not observe any significant differences in fractional anisotropy (FA) values in the neocortex or hippocampal regions but did observe significant changes in the CC (Fig. 3B). In SL controls, the FA values showed a normal increase with age (Semple et al., 2013; Wang et al., 2009). However, in HA mice there were no differences between FA in the CC at 1 month of exposure or any of the remaining time points. The divergence of these two trends became significant by 3 months. These results suggest either a prevention of normal maturation of myelination and/or de- or dysmyelination in the white matter of HA mice.

In contrast to FA, mean diffusivity (MD) values were significantly elevated in neocortex, CC and hippocampus after three months of HA exposure and remained elevated after ≥6 months of exposure in the neocortex (Fig. 3C). To delineate the changes in MD, axial and radial diffusivity (AD/RD) were evaluated. We did not find any significant changes in AD or RD values at 1 month in neocortex or hippocampus of HA exposed or SL mice (Fig. 3D and E). However, after 3 months, MD,

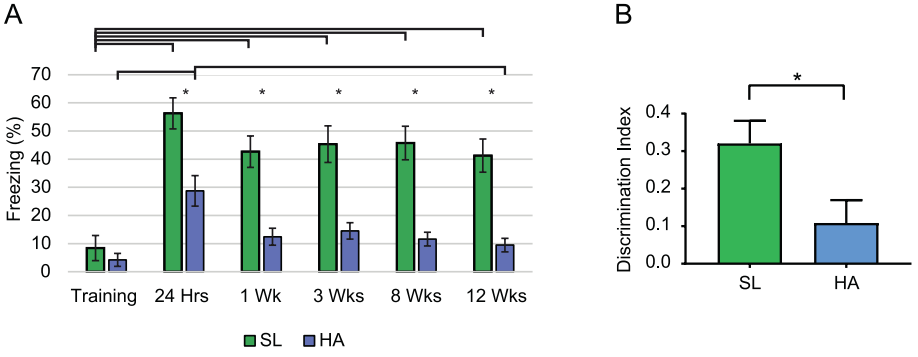

Fig. 1. Mice exposed to HA show hippocampal related deficits in contextual memory formation.
(A) Bar graph depicting the percentage of time spent freezing in a fear conditioning protocol during the first 2 minutes (pre-shock period) over the course of repeated exposures. Prior to the shock (training) there was no significant difference between HA and SL mice. However, compared to SL, HA mice spent significantly less time freezing when returned to the context 24 h later. This difference persisted over a 12-week exposure period by which time HA mice had returned to pre-shock levels of freezing while SL mice maintained a stable degree of freezing throughout the 12-week measurement period. Note that exposure time to HA is 3-weeks plus the time indicated. * = $p < .001$, Two-way repeated measures ANOVA with Holm-Sidak post-hoc comparison. $N = 8$ mice for all groups at each time point. (B) Three-month exposed HA mice also fail to form strong object-context associations relative to SL controls as evidenced by a lower discrimination index in the novel object recognition test. $N = 12$ SL and $N = 13$ HA per group, $p = .021$ unpaired Student's *t*-test.

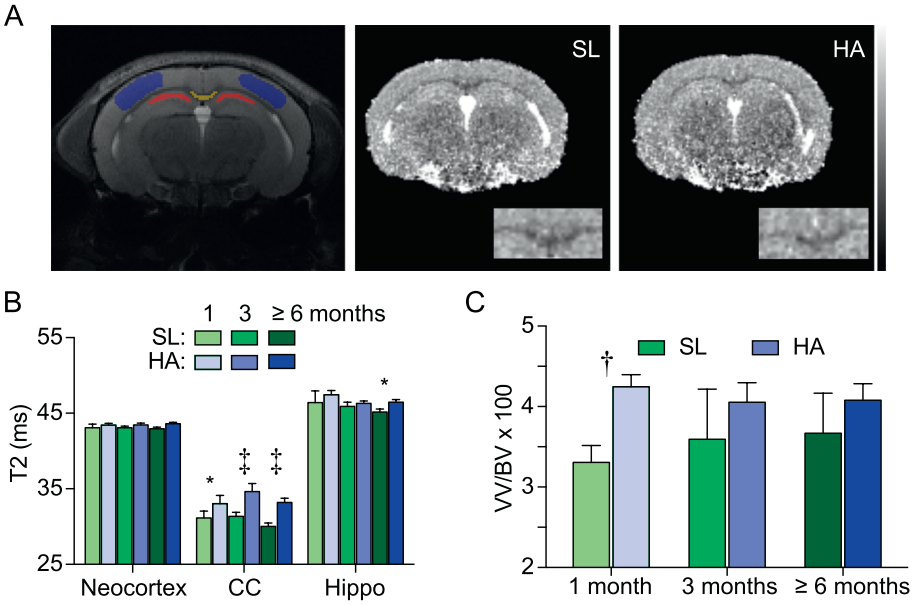

Fig. 2. MRI T2 relaxation times are increased in selected brain regions following HA exposure.
(A) Representative T2-weighted image indicating analysis ROIs and T2 maps for a SL and HA mouse scaled 10 to 60 ms. Insets show representative values for the corpus callosum. (B) T2 values in different brain regions and normalized ventricular volume (C) calculated for 1, 3, and 6 months HA and SL animals. T2 values are particularly elevated in the corpus callosum with observable increases in normalized VV for HA exposed animals. Two-way ANOVA for T2 values and *t*-test for nVV: * = $p < .05$, † = $p < .01$, ‡ = $p < .001$. Number of mice were: 1 month: 3 SL and 3 HA; 3 months: 4 SL, and 3 HA; 6+ months (6 and 8 months combined): 5 SL and 5 HA.

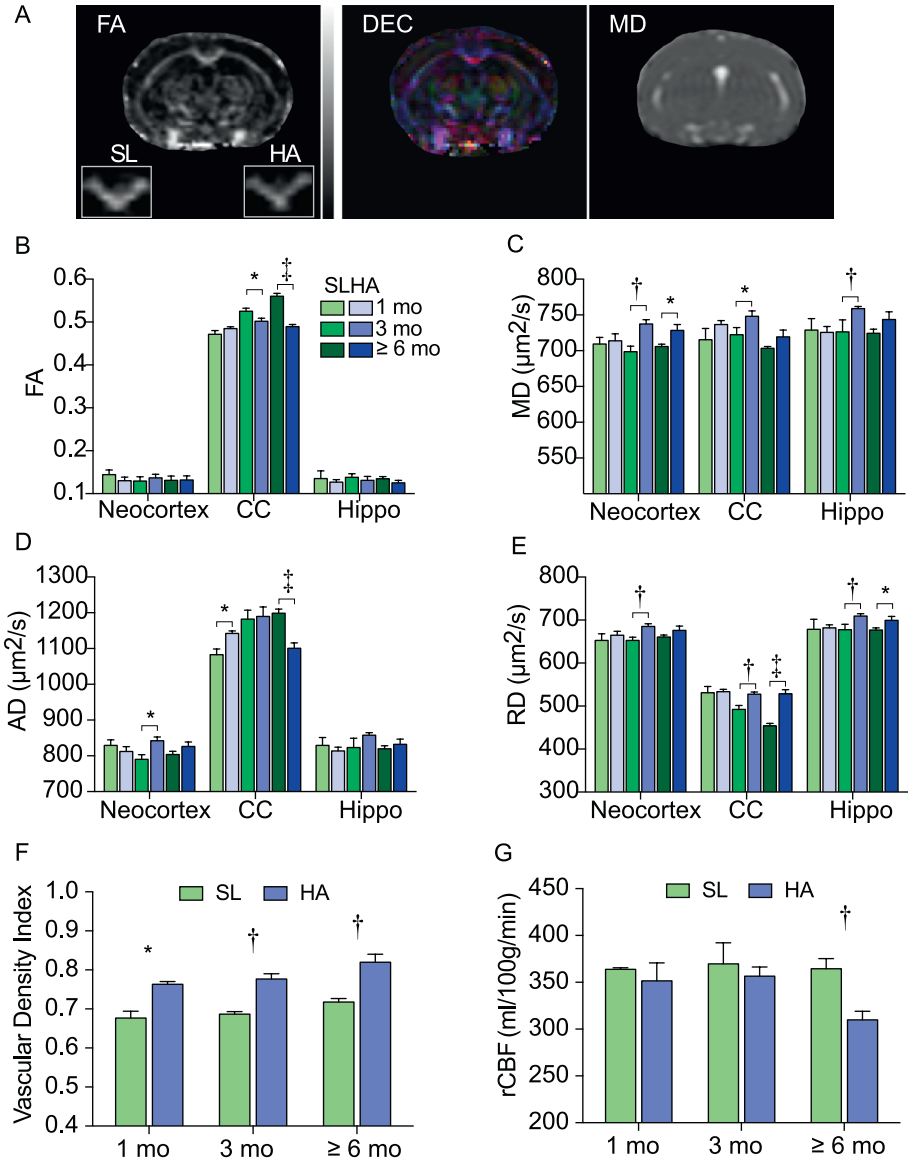

Fig. 3. Fractional anisotropy of white matter decreases, whereas vascular density index and cerebral blood flow are impacted following HA exposure.
(A) Typical DTI derived diffusion index maps such as Fractional Anisotropy scaled from 0 to 1 (with representative images from the CC as insets), directionally-encoded color FA (DEC FA), and Mean Diffusivity maps. (B) FA values didn't show significant differences in neocortex and hippocampus regions. There is a significant drop of FA in CC at 3 and ≥6 months of exposure to HA. There is an increase of MD values (C) across all brain regions in animals exposed to HA conditions at 3 months and, in the neocortex, at 6 months. Significant reduction of axial diffusivity (AD, panel D) with elevated radial diffusivity (RD, panel E) in CC at later time points suggesting demyelination, edema, and/or neuroinflammation. Two-way ANOVA: * = $p < .05$, † = $p < .01$, ‡ = $p < .001$. Changes in vascular density index (VDi, panel F) and relative cerebral blood flow (rCBF, panel G) in the neocortex of HA and age matched SL control mice show significant differences in both measures. HA mice changes are consistent with higher blood vessel densities but lower rCBF compared to SL animals. t-test: * = $p < .05$, † = $p < .01$, ‡ = $p < .001$. Number of mice were: 1 month: 3 SL and 3 HA; 3 months: 4 SL, and 3 HA; 6+ month: 5 SL and 5 HA.

AD and RD values were higher in neocortex in HA mice compared to SL consistent with an ongoing neuroinflammatory process. In the CC at 3 months, MD and RD increased with a corresponding decrease in FA. These patterns of diffusion measures may reflect axonal degeneration and/or demyelination. In the SL group white matter maturation was evident from increasing FA and AD with decreasing RD over the 6-month observation period.

3.2.2. Vascularization and blood flow

Vasogenic edema has been proposed to play a significant role in the neuropathology of HA exposure (Hackett et al., 1998) and changes in the vasculature structure and function may critically impact the cognitive changes. To obtain an in vivo measure of hypobaric-hypoxia induced cerebrovascular changes, a vascular density index (VDi) was derived from a pre- and post-contrast Magnetic Resonance Angiography (MRA). The calculated VDi of the neocortex (Fig. 3F) was elevated in HA mice in all exposed groups beginning at 1 month consistent with chronic hypobaric-hypoxia driven increases brain vascularity.

Cerebral blood flow (CBF) serves as an indicator of cerebral metabolism and provides insight into oxygenation capacity of the vascular network in the brain. Relative cerebral blood flow (rCBF) remained unchanged in HA exposed animals relative to SL controls up to 3 months of exposure. However, after 6 months of continuous exposure to HA conditions, rCBF was reduced in HA exposed mice (Fig. 3G).

Since adaptive changes in vasculature may include changes in the hematocrit in response to hypoxic conditions we measured hematocrit levels. Previously we reported that a three week exposure to HA causes a significant increase in the hematocrit of C57Bl6/J mice from 53.4 ± 0.4% in controls to 78 ± 1% in exposed mice (Cramer et al., 2015). Here we extended the hematocrit measurements and found that after 2 months of exposure, the hematocrit of HA mice was 81 ± 1% ($n = 4$) compared to 51 ± 1% (n = 4) in SL controls. We re-examined the hematocrit in a subset of HA mice after 3 months exposure and found no significant increase from those at the 2-month exposure period (80.9 ± 0.9%, $n = 3$). In comparison, the hematocrit for age-matched SL controls remained low at 57 ± 1% ($n = 5$). This increase in hematocrit may affect blood viscosity and contribute to the lower rCBF values in HA mice (Fig. 3G).

3.3. HA exposure increases neurovascular density

Given the capacity for the vasculature to adapt to chronic hypoxia (Ainslie and Ogoh, 2010; Willie et al., 2015) and our observation of elevated VDi in the neocortex (Fig. 3), we began by investigating changes in cerebrovasculature. Representative images of the vasculature are shown in Fig. 4A. Quantification of the percentage of area taken up by the vasculature revealed significant increases in HA mice relative to SL in the neocortex, CC and hippocampus (Fig. 4B: neocortex: 4.2 ± 0.1% in control versus 5.5 ± 0.4% in HA, $p = .015$; CC: 2.1 ± 0.1 in control versus 3.1 ± 0.2 in HA, $p = .013$; hippocampus: 3.1 ± 0.2 in SL versus 4.6 ± 0.2 in HA, $p = .004$: n = 5 and 4 for SL and HA respectively). Additionally, when normalized to control mice, the hippocampal parenchyma of HA mice had significantly elevated albumin staining consistent with disruption of the blood-brain barrier (BBB) (relative optical densities of 1.0 ± 0.04 for SL vs. 1.4 ± 0.1 for HA, $n = 7$ per group. $p = .026$ Mann-Whitney test; Supplemental Fig. 1). Therefore, consistent with our observation of increased VDi in the neocortex (Fig. 3), we find significant expansion of the vascular network in all investigated brain regions, which may have diminished BBB integrity.

3.4. Altered myelination correlates with functional changes within the corpus callosum

In order to parallel MRI findings with regard to myelination, we assessed the degree of myelination in the CC using LFB staining

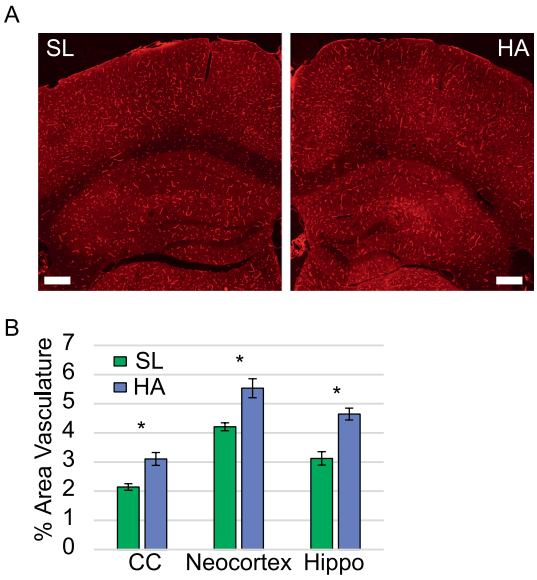

Fig. 4. HA exposure induced angiogenesis in the brain.
(A) Representative images of coronal brain sections from a control SL mouse (left) and a HA mouse (right) after 3 months of exposure. The vasculature was labeled by tail vein injection of lectin-conjugated dye. (B) Group data from SL ($n = 5$) and HA ($n = 4$) mice reveal a significant increase in vascularization following HA exposure (* = $p < .05$, Student's t-test).

(Fig. 5A). Similar to MRI observations, the intensity of LFB staining within the CC was significantly lower in HA exposed mice (as evidenced by a higher cumulative probability of brighter pixel intensities resulting from reduced myelin within the CC; Fig. 5B, $p < .0001$, n = 4 per group; Kolmogorov-Smirnov test), further suggesting deficits in myelination (Deshmukh et al., 2013).

The functionality of the CC was assessed in 8 SL and 7 HA mice by measuring compound action potential (CAP) conduction kinetics ex vivo. CAP velocities were not significantly different in either the myelinated component (N1: 1.06 ± 0.03 m/s versus 1.11 ± 0.04 m/s for SL and HA respectively; $P = .8$ Student's t-test) or unmyelinated component (N2: 0.38 ± 0.02 m/s versus 0.36 ± 0.02 m/s for SL and HA respectively; Student's t-test, $p = .9$, Fig. 5D). However, the input-output relationships, which provide a measure of the recruitment levels of N1 and N2 contributing fibers as a function of action potential activation threshold, were significantly increased by HA exposure. Representative examples of CAP evoked by an identical range of stimulation intensities for SL and HA exposed mice are shown in Fig. 5C, while group data for SL and HA mice are shown in Fig. 5E & F for myelinated (N1) and unmyelinated (N2) fibers, respectively. In addition, the ratio of N1 to N2 amplitudes was significantly reduced (Fig. 5G) while refractory periods were increase (Supplemental Fig. 2) in HA mice. Therefore, augmented N1 and N2 responses for both myelinated (faster conducting) fibers and unmyelinated (slower conducting) fibers (Fig. 5E and F) results in an abnormal recruitment pattern for stimulation of CC following HA exposure.

3.5. Microglia show increased phagocytic activity following hypobaric-hypoxia

We hypothesized that a microglia mediated inflammatory microenvironment triggered by hypobaric hypoxia (Boos et al., 2016; Kubo et al., 1998; Lemos et al., 2013) could contribute to vascular remodeling and myelination deficits. Representative images of endogenous GFP expression by microglia and CD68 immunoreactivity, a marker of lysosomal activity, are shown in Fig. 6A. Quantification of the microglia densities within the three primary regions of interest

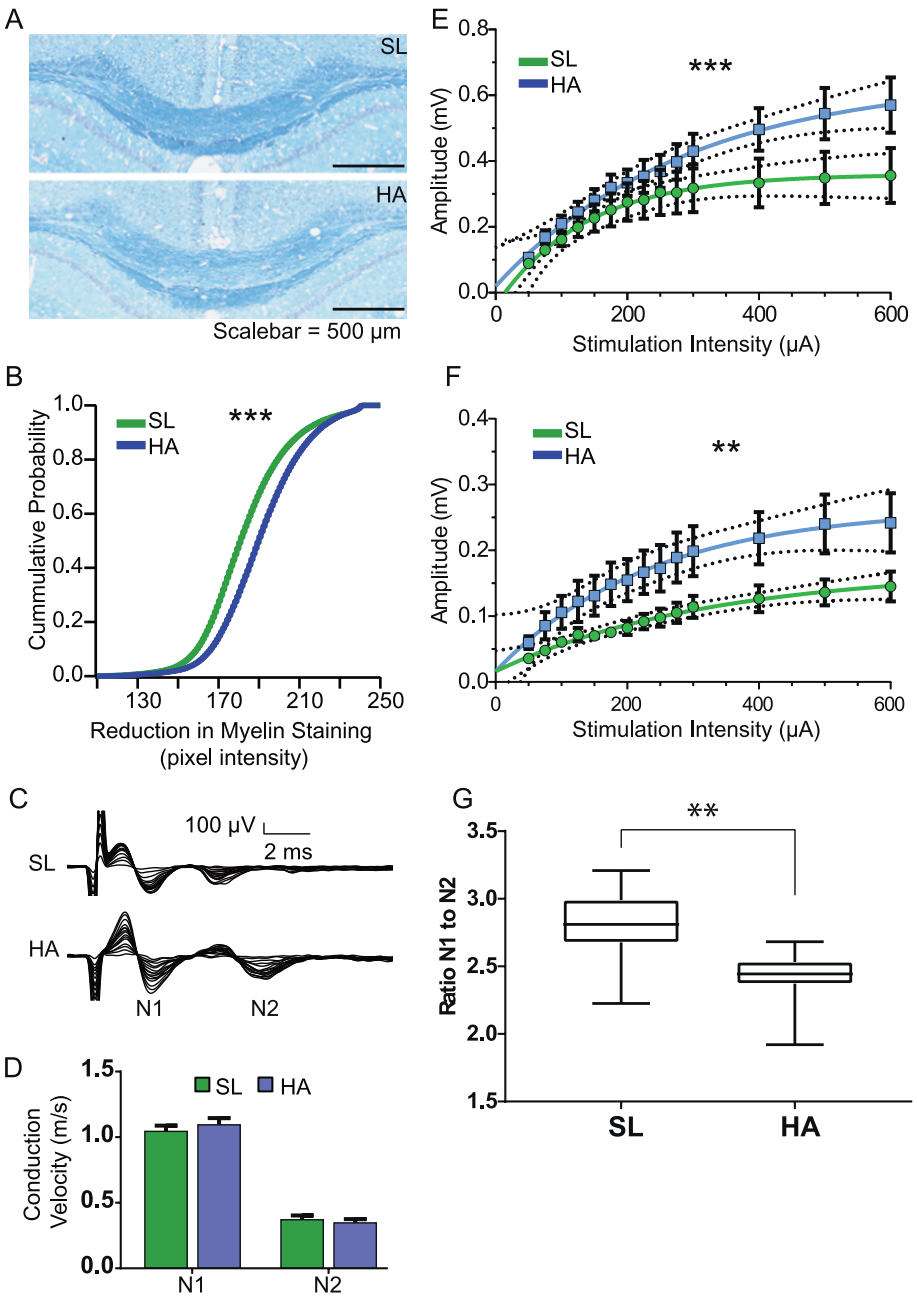

Fig. 5. HA exposure reduces myelination but enhances excitability in the corpus callosum.
(A) Representative images showing reduced LFB staining in coronal brain section of a SL (top) and HA (bottom) mouse. (B) Quantification on paired cut and stained brains (SL and HA) of pixel intensities in n = 4 mice from each group revealed that the pixel intensities are significantly brighter (less blue) in HA mice than SL indicating less myelination ($p < .05$, Kolmogorov–Smirnov test) on paired brains. (C) Representative CAP waveforms in response to a range of stimulation intensities for SL (top) and HA mice (bottom). (D) Conduction velocities for myelinated (N1) and unmyelinated (N2) fibers were not significantly changed by HA exposure ($n = 8$ for SL and $n = 7$ for HA). Input output relationship group data (n = 8 for SL and n = 7 HA) for myelinated (E) and unmyelinated fibers (F) reveal that both fiber types are more excitable in HA mice than SL mice. Contributions from unmyelinated fibers are larger in HA mice as evidenced by a smaller N1/N2 amplitude ratio (G) ** = $p \leq .001$, *** = $p < .0001$; Comparison of nonlinear fit decay constants (E and F) or Student's t-test (D and G). (For interpretation of the references to color in this figure legend, the reader is referred to the web version of this article.)

revealed no significant differences between conditions (Fig. 6B: SL vs HA: neocortex, 109 ± 5 vs 109 ± 4 per mm^2, $p = .7$; CC, 96 ± 8 vs 91 ± 8 per mm^2, $p = .68$; hippocampus, 118 ± 8 vs 104 ± 8 per mm^2, $p = .22$; Student's *t*-test, $n = 8$ SL and HA mice per group). Although the densities of microglia where not significantly different between the two conditions, microglia from HA exposed mice tended to have significantly greater CD68 loads within the cell bodies (calculated as percent CD68 signal per microglia cellular area, Fig. 6C-E). This suggests that microglia in HA mice are more actively involved in phagocytosis than in SL mice in all examined regions.

3.6. Hippocampal and amygdala transcriptomes exhibit signatures of hypobaria and hypoxia

We used RNA-Seq mediated transcriptional analysis on C57Bl6/J hippocampi and amygdalae in order to obtain molecular insight into time-dependent changes in regulatory and signaling pathways following 3 and 12 weeks of HA exposure (see Supplemental Fig. 3 for a representative IGV track). The reads mapped to exons of 38,484 transcripts and the pools of transcripts in both hippocampus and amygdala samples were distinct.

The Venn diagram (Fig. 7A) illustrates our results, which are detailed in Supplemental Table 1. We identified 200 differentially expressed transcripts in the hippocampus and 176 in the amygdala following 3-week HA exposure, 32% of the identified amygdalar transcripts (56/176) overlap between tissues.

Following 12-week HA exposure, 71 and 33 differentially expressed transcripts were found in the hippocampus and amygdala respectively, 58% of amygdalar (19/33) differentially expressed transcripts were also identified in the hippocampus (Fig. 7A and Supplemental Fig. 4, Supplemental Table 1). We identified 12 differentially expressed transcripts in all tissues at all timepoints; all were linked to vascular plasticity and remodeling of BBB (Right panel, Fig. 7A).

Volcano plots skew towards transcriptional induction rather than

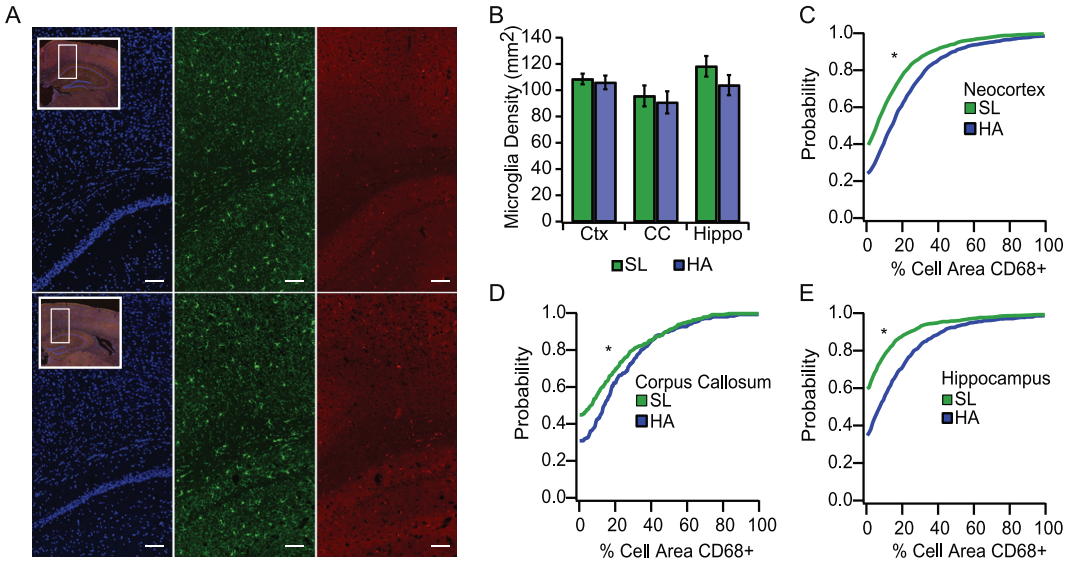

Fig. 6. Enhanced microglia phagocytic activity in HA exposed mice.
(A) Representative images of coronal brain sections showing portions of the neocortex, corpus callosum and hippocampus from SL control (top row) and 3-month HA exposed (bottom row) mice. Images left to right show DAPI stained nuclei (blue), endogenous GFP expression driven by the *Cx3cr1* gene in microglia (green) and CD68 (a marker of phagocytic activity, red). The inset in each row shows a larger view of the representative section with the white rectangle indicating the expanded region. Scale bar = 100 μm. (B) Quantification of the density of microglia in these three regions was not significantly different (Student *t*-test, $p > .05$; n = 8 mice for SL and $n = 6$ mice for HA). Probability distribution curves for the percent area of microglia soma that is CD68 immunopositive in the neocortex (C), corpus callosum (D) and hippocampus (E) are shifted to the right in HA mice suggesting that microglia from HA exposed mice have a greater lysosome load than those from SL mice in all three regions. (For interpretation of the references to color in this figure legend, the reader is referred to the web version of this article.)

suppression for hippocampus and amygdala (Fig. 7B-C and Supplemental Fig. 4). Upregulated transcripts (i.e. xanthine dehydrogenase (Xdh), ATP-binding cassette, sub-family B, member 1A (Abcb1a), lymphocyte antigen 6 complex, locus C1 (Ly6c1), solute carrier organic anion transporter family, member 1a4 (Slco1a4), flavin containing monooxygenase 2 (Fmo2), regulator of G-protein signaling 5 (Rgs5), vitronectin (Vtn) and chemokine (C-X-C motif) ligand 12/stromal cell-derived factor 1 (Cxcl12/SDF1)) are largely related to vascular development, BBB formation and inflammation. Although we observe ontological enrichment of transcripts associated with neurological function at 3- and 12-weeks, the differential expression of factors directly impacting neurological function occurs primarily at the 3-week time point (Fig. 7D).

We performed real-time PCR for selected targets as validation of transcriptomics results. qPCR analysis of the transcripts Cxcl12, Flt1, Vtn, Fn1 and Vwf confirmed increased expression in the hippocampus following 12 weeks high altitude exposure, as initially identified through RNA-Seq (Supplemental Table 1). The ratios of HA to SL transcript expression fold changes were (mean ± SEM): Cxcl12: 1.32 ± 0.09, $p = .053$; Flt1: 1.44 ± 0.07, $p = .015$; Vtn: 1.43 ± 0.04, $p = .0002$; Fn1: 1.67 ± 0.10, $p = .001$; Vwf: 2.35 ± 0.13, $p = .0003$ (n = 5 HA and 5 SL).

4. Discussion

Performing long-term operations, working and/or living in the hypobaric-hypoxic conditions at HA, including space exploration, can have significant physiological impacts affecting exercise performance, operational and mental capabilities (Anderson et al., 2011; Cowell et al., 2002; De Peuter et al., 2004; Fan and Kayser, 2016; Smith, 2005; Waligora et al., 1991). Using our mouse model which mimics HA induced memory deficits, we investigated the mechanisms underlying these changes. In line with cognitive deficits observed in humans (Abraini et al., 1998; Ryn, 1979, 1988; Subudhi et al., 2014) and rats (Maiti et al., 2008; Titus et al., 2007) after HA exposure, we found that mice which resided at a simulated elevation of 5000 m showed evidence of poorer spatial memory formation and retention compared to SL controls (Fig. 1). This result suggests that chronic HA exposure impairs both spatial (declarative) memory formation and retention.

MR imaging of the neocortex, CC and hippocampus from similarly exposed mice revealed that T2 values increased most prominently in the CC as a function of exposure duration relative to age matched SL controls. Increased T2 value are consistent with HACE pathology in humans and may be an indication of vasogenic edema (Hackett et al., 1998) or ongoing inflammatory processes. In our study, the changes occurred relatively early during the first month of HA exposure and continue into later time points suggesting either chronic inflammation or persistent structural changes. DTI metrics, which can provide insights into structural changes, were also altered in the CC as well as the hippocampus of HA exposed mice. Fractional anisotropy was lower than SL controls after 3 months at altitude, a change that was largely due to elevated radial diffusivity. A similar pattern of increased radial diffusivity with relatively normal axial diffusivity has been correlated with myelination deficits in the shiverer mouse (Song et al., 2002) and hypoxic-ischemic damage to myelination in the neonatal rat brain (Wang et al., 2009). When coupled with increased microglia phagocytic activity (Fig. 6), decreased luxol fast blue staining and altered fiber excitability (Fig. 5), these results suggest microglia may contribute to hypobaric-hypoxia induced reduced myelination/demyelination, increased excitability of the CC, and impaired hippocampal function. Our electrophysiological results are consistent with increased excitability in fast and slow axons in the CC following HA exposure and can be paralleled to increased firing activity found in aged rhesus monkey prefrontal cortex neurons (Coskren et al., 2015). Decreased N1/N2 ratios suggest a bigger impact on excitability in slower unmyelinated fibers whereas a longer refractory period reflects axonal damage and/or suggests changes in inactivation gating of sodium channel for both fast and slow components (Bucher and Goaillard, 2011; Colley et al., 2010; Mangiardi et al., 2011). We can speculate that changes in myelination patterns can be an adaptive mechanism that ensures a normal AP conduction velocity.

At all time-points, we see ontological evidence of increased

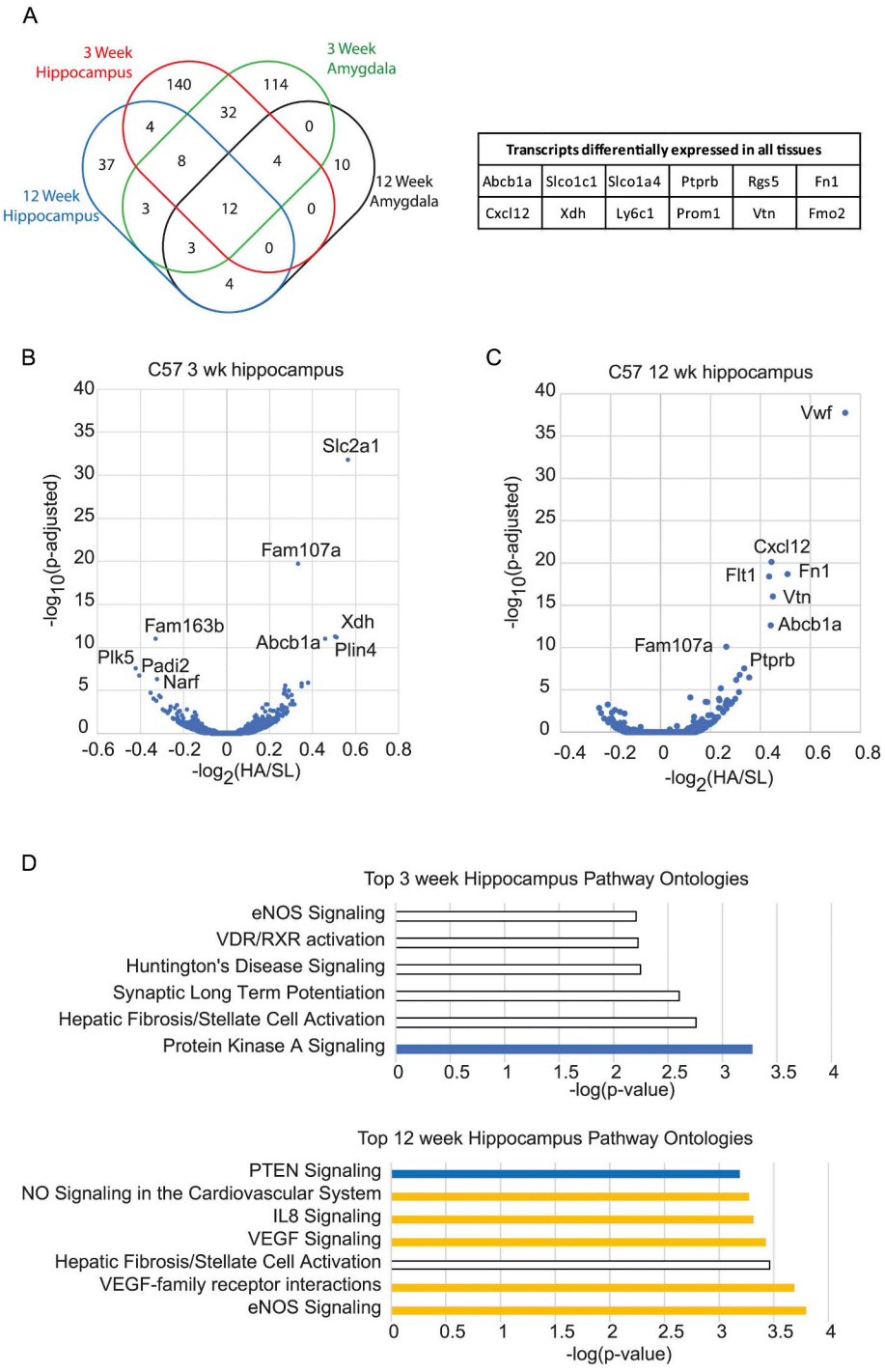

Transcripts differentially expressed in all tissues					
Abcb1a	Slco1c1	Slco1a4	Ptprb	Rgs5	Fn1
Cxcl12	Xdh	Ly6c1	Prom1	Vtn	Fmo2

Fig. 7. Hippocampal transcriptome following 3- and 12- week HA exposure.
(A) Left panel: Venn Diagram of differentially expressed transcripts (p-adjusted < 0.1) in the 3-week and 12-week exposed hippocampus and amygdala. A total of 286 transcripts were differentially expressed following 3-weeks, but not 12 weeks, of HA exposure, with 32 of these transcripts altered in both the hippocampus and amygdala. Only 51 transcripts were differentially expressed following 12-weeks, but not 3 weeks, of HA exposure, with only 4 of these transcripts altered in both tissues. Right panel: The table lists the 12 differentially expressed transcripts common to both brain regions and time points. (B, C) Volcano plots for all hippocampal transcripts following the 3- and 12-week exposures. Transcripts differentially expressed in response to HA exposure for all time points and tissues skew towards upregulation rather than downregulation. (D) Bar plots showing biological pathways associated with differentially expressed transcripts after 3-weeks and 12-weeks of HA exposure for the hippocampus. Pathway induction is in orange, suppression is in blue, and uncertain/not applicable direction is in white. Number of mice/samples were: 3-weeks (5 SL and 5 HA); 12-weeks (5 SLs and 5 HA). Gene abbreviations, which were not mentioned in the Methods or Result section: solute carrier organic anion transporter family, member 1c1 (Slco1c1); protein tyrosine phosphatase, receptor type, B (Ptprb); prominin 1 (Prom1); polo-like kinase 5 (Plk5); peptidyl arginine deiminase, type II (Padi2); family with sequence similarity 163, member B (Fam163b); nuclear prelamin A recognition factor (Narf); solute carrier family 2 (facilitated glucose transporter), member 1 (Slc2a1); family with sequence similarity 107, member A (Fam107a); perilipin 4 (Plin4). (For interpretation of the references to color in this figure legend, the reader is referred to the web version of this article.)

angiogenesis/vasculature and inflammation in our RNA-Seq data. In particular, the prominent transcripts upregulated in the 3 week hippocampus (Fig. 7) suggest the brain may still be adapting to the metabolic stress resulting from decreased oxygen availability. Slc2a1 encodes a glucose transporter that shuttles glucose across the BBB and between glia (Zhao and Keating, 2007) and is a downstream target of HIF-1α (Nayak et al., 2016). Its upregulation at 3 weeks suggests the brain is still under significant metabolic stress. Indeed, our observation of Fam107a upregulation in the hippocampus has also been reported in a model of neonatal stress where reduced dendritic density with aberrant LTP in the CA1 region of the hippocampus was also observed (Schmidt et al., 2011). At 12 weeks, the more prominently upregulated transcripts include those regulated by HIF-1α or VEGF related to blood brain barrier permeability and angiogenesis (Vwf, Flt1, Vtn, Fn1 and Cxcl12) (Benito-Jardon et al., 2017; Chappell et al., 2013; Mathew et al., 2017; Real et al., 2011; Selvaraj et al., 2017; Stowe et al., 2011; Suidan et al., 2013). Indeed, upregulation of Cxcl12 has been linked to increase BBB permeability (Selvaraj et al., 2017; Huang et al., 2013; Man et al., 2012; McCandless et al., 2009) as observed in our study (Supplemental Fig. 1). Additionally, Fam107a remains upregulated at this later time point, suggesting that, despite adaptations in the vasculature, hippocampal networks remain under significant stress.

RNA-Seq analysis of hippocampal tissue also provided insight into the possible underlying mechanisms contributing to maladaptation to HA. Padi2, which encodes one of five isoforms of peptidyl arginine deiminases, is downregulated in the HA exposed hippocampus (Padi2;

Supplemental Table 1, Fig. 7B-C). PAD catalyzes post-translational citrullination of proteins, including myelin basic protein, and is implicated in the pathogenesis of MS and AD (Chirivi et al., 2013; Gyorgy et al., 2006). This result indicates hypobaric-hypoxia modifies pathways involved in myelination and axonal excitability. Narf, another transcript downregulated by HA exposure, appears to play a role in hippocampal synaptic plasticity as it is upregulated by strong synaptic activity in the hippocampus and cerebellum, localizes to neurites and associates with myosin V (Ohkawa et al., 2001), a protein involved in receptor trafficking and LTP induction (Kneussel and Wagner, 2013). Its reduction in HA-exposed mice is consistent with deficits in hippocampal mediated memory formation (Fig. 1). Metabotropic glutamate receptor 3 (GRM3), which is critical for performance in forced swim tests, cued and contextual fear conditioning, and the T-maze forced alternation test (Fujioka et al., 2014), has its transcript Grm3 downregulated at the 3-week time point in the amygdala. By contrast, there were far fewer neurological-related transcripts differentially expressed at the 12-week time point. Furthermore, these transcripts appeared to be primarily glial in nature. Slc1a3, a glutamate-aspartate transporter highly expressed in glia (Hagiwara et al., 1996), and Glul, a glutamine synthetase associated with glutamate recycling in glia (Eid et al., 2013), have transcripts that are both upregulated in the hippocampus, suggesting induction of potential protective mechanisms against glutamate mediated neurotoxicity.

Inflammation/angiogenic alterations at the 3-week time point are primarily associated with the extracellular matrix (transcripts encoding: Fn1 and Col11a2), proliferation-associated growth factor signaling (transcripts encoding: insulin-like growth factor binding protein 7 (Igfbp7), and Igfb3, insulin-like growth factor I receptor (Igf1r), and stress responses (transcripts encoding: heat shock protein 5 (Hspa5) and Fam107a). By contrast, the top 12-week hippocampus ontology categories associated with inflammation and angiogenesis are predominantly vasculature associated, including VEGF-related receptors (transcripts encoding: Flt1, Flt4 and kinase insert domain protein receptor (Kdr), along with transcripts endothelial-specific receptor tyrosine kinase (Tek), nitric oxide related nitric oxide synthase trafficker (Nostrin) and nitric oxide synthase 3, endothelial cell (Nos3), and leukocyte migration-associated Cxcl12 and platelet/endothelial cell adhesion molecule 1 (Pecam1). However, Igfbp7 and Flt1 remain upregulated in both hippocampus and amygdala as well.

It is interesting to mention that commercial flights are only pressurized to not exceed 8000 ft (Affleck et al., 2008) where the inspired PO_2 is approximately 75% of its sea level value (West, 2004). While our experiments simulate much higher altitude (5000 m with an inspired PO_2 of approximately 52% of the sea level value), the complexity of the response would suggest that it is worthwhile to look at the extent to which these observations extend to repeated low-to-moderate altitude exposure, as would be seen for frequent fliers, commercial and military flight crews and exposure during space exploration missions.

In conclusion, our study unravels impaired hippocampus-mediated learning and memory following chronic HA exposure. Hypobaric-hypoxia drives vascular remodeling and functional and structural changes in white matter myelination. When combined with an increased inflammatory tone and probable channelopathies in affected neurons, these neuropathological mechanisms contribute to long-lasting cognitive deficits. The structural and functional changes we observed in the CC suggest that the mechanisms contributing to altered excitability of myelinated and unmyelinated fibers may arise from systemic extrinsic factors driven by HA-induced vascular changes. Our results also suggest that microglia may play a mediatory role between vascular remodeling induced by HA exposure and subsequent neuropathologies. However, further research is needed to determine whether microglia activation is truly causal or a secondary response to hyobaric-hypoxia. Importantly, our transcriptomics analysis identified sets of targets to be pursued in future studies which may play a causative role in brain adaptation during HA exposure.

Acknowledgments

We thank Dr. Manoj Jaiswal (APG/CNRM, USUHS), Drs. Dinesh Shukla and Reed Selwyn (CNRM, USUHS), Dr. Charles A. Vacchiano (Duke University) and Dr. Richard T. Mahon (Undersea Medicine Department, Naval Medical Research Center) for their help and inspiration at the beginning of this project. We also thank Mr. Stephen Reimers, Reimers Systems, Inc. for all his outstanding work related to the design and construction of our hypobaric chamber. We also would like to express our gratitude to Drs. Sharon Shively, Dara Dickstein, Diego Iacono and Daniel Perl (Dept. Pathology, School of Medicine, USUHS) for countless discussions and comments during the progress of this work and on manuscript and Dr. Regina Armstrong (Dept. Anatomy, Physiology and Genetics, USUHS) for her insightful feedback during the manuscript preparation.

We would like to thank Dr. Caroline Browne (Dept. Pharmacology and Molecular Therapeutics, USUHS) for her expert help and suggestions on novel object recognition data analysis and interpretation.

Competing financial interests

The authors declare no competing financial or commercial conflict of interests.

Support

This research was partially supported by a grant from the Air Force Medical Support Agency, U.S. Department of Defense, Program Project 308430 USUHS, and Collaborative Health Initiative Research Program (NHLBI/NIH and USUHS). Support for this work also included funding from the U.S. Department of Defense in the Center for Neuroscience and Regenerative Medicine (CNRM).

Disclaimer

The views expressed in this scientific presentation are those of the author(s) and do not reflect the official policy or position of the U.S. government or the Department of Defense.

Appendix A. Supplementary data

Supplementary data to this article can be found online at https://doi.org/10.1016/j.expneurol.2018.10.007.

References

Abraini, J., Bouquet, C., Joulia, F., Nicolas, M., Kriem, B., 1998. Cognitive performance during a simulated climb of Mount Everest: implications for brain function and central adaptive processes under chronic hypoxic stress. Pflügers Arch. Eur. J. Physiol. 436, 553–559. https://doi.org/10.1007/s004240050671.

Affleck, J., Angelici, A., Baker, S., Brook, T., Cimrmancic, M., Cocks, R., Dejohn, C., Eldredge, L., Elliott, J., Evans, T., Feeks, E., Fox, K., Fraser, J., Hall, P., Heupel, K., Kakimoto, Y., Kyff, J., Lewis, M., Li, G., Luna, T., Maclarn, G., Marsh, R., McKeon, J., Mera, E., Moore, V., Muhm, M., Musselman, B., Murdoch, D., Ostrander, G., Pascoe, G., Ricaurte, E., Ritter, D., Ryan, R., Sahiar, F., Salazar, B., Sardana, T., Shanahan, D., Sky, J., Smart, T., Stepane, J., Villaire, N., Webster, N., White, D., Wolbrink, A., Woodrow, A., Wood, R., Wurmstein, A., Zarr, S., 2008. Cabin cruising altitudes for regular transport aircraft. Aviat. Space Environ. Med. 79, 433–439.

Ainslie, P.N., Ogoh, S., 2010. Regulation of cerebral blood flow in mammals during chronic hypoxia: a matter of balance. Exp. Physiol. 95, 251–262. https://doi.org/10.1113/expphysiol.2008.045575.

Anders, S., McCarthy, D.J., Chen, Y., Okoniewski, M., Smyth, G.K., Huber, W., Robinson, M.D., 2013. Count-based differential expression analysis of RNA sequencing data using R and Bioconductor. Nat. Protoc. 8, 1765–1786. https://doi.org/10.1038/nprot.2013.099.

Anderson, P.J., Miller, A.D., O'Malley, K.A., Ceridon, M.L., Beck, K.C., Wood, C.M., Wiste, H.J., Mueller, J.J., Johnson, J.B., Johnson, B.D., 2011. Incidence and symptoms of high altitude illness in south pole workers: antarctic study of altitude physiology (ASAP). Clin. Med. Insights. Circ. Respir. Pulm. Med. 5, 27–35. https://doi.org/10.4137/CCRPM.S6882.

Antunes, M., Biala, G., 2012. The novel object recognition memory: neurobiology, test

procedure, and its modifications. Cogn. Process. https://doi.org/10.1007/s10339-011-0430-z.
Appenzeller, O., Passino, C., Roach, R., Gamboa, J., Gamboa, A., Bernardi, L., Bonfichi, M., Malcovati, L., 2004. Cerebral vasoreactivity in Andeans and headache at sea level. J. Neurol. Sci. 219, 101–106. https://doi.org/10.1016/j.jns.2003.12.014.
Benito-Jardon, M., Klapproth, S., Gimeno-Lluch, I., Petzold, T., Bharadwaj, M., Muller, D.J., Zuchtriegel, G., Reichel, C.A., Costell, M., 2017. The fibronectin synergy site re-enforces cell adhesion and mediates a crosstalk between integrin classes. elife 6. https://doi.org/10.7554/eLife.22264.
Boos, C.J., Woods, D.R., Varias, A., Biscocho, S., Heseltine, P., Mellor, A.J., 2016. High altitude and acute mountain sickness and changes in circulating endothelin-1, interleukin-6, and interleukin-17a. High Alt. Med. Biol. 17, 25–31. https://doi.org/10.1089/ham.2015.0098.
Bucher, D., Goaillard, J.-M., 2011. Beyond faithful conduction: short-term dynamics, neuromodulation, and long-term regulation of spike propagation in the axon. Prog. Neurobiol. 94, 307–346. https://doi.org/10.1016/j.pneurobio.2011.06.001.
Cavaletti, G., Garavaglia, P., Arrigoni, G., Tredici, G., 1990. Persistent memory impairment after high altitude climbing. Int. J. Sports Med. 11, 176–178. https://doi.org/10.1055/s-2007-1024787.
Chappell, J.C., Mouillesseaux, K.P., Bautch, V.L., 2013. Flt-1 (vascular endothelial growth factor receptor-1) is essential for the vascular endothelial growth factor-Notch feedback loop during angiogenesis. Arterioscler. Thromb. Vasc. Biol. 33, 1952–1959. https://doi.org/10.1161/ATVBAHA.113.301805.
Chen, J., Fan, C., Li, J., Han, Q., Lin, J., Yang, T., Zhang, J., 2016. Increased intraregional synchronized neural activity in adult brain after prolonged adaptation to high-altitude hypoxia: a resting-state fMRI study. High Alt. Med. Biol. 17, 16–24. https://doi.org/10.1089/ham.2015.0104.
Chirivi, R.G.S., Van Rosmalen, J.W.G., Jenniskens, G.J., Pruijn, G.J., Raats, J.M.H., 2013. Citrullination: a target for disease intervention in multiple sclerosis and other inflammatory diseases? J. Clin. Cell. Immunol. 4. https://doi.org/10.4172/2155-9899.1000146.
Clasen, R.A., Pandolfi, S., Hass, G.M., 1970. Vital staining, serum albumin and the blood-brain barrier. J. Neuropathol. Exp. Neurol. 29, 266–284.
Claydon, V.E., Gulli, G., Slessarev, M., Appenzeller, O., Zenebe, G., Gebremedhin, A., Hainsworth, R., 2008. Cerebrovascular responses to hypoxia and hypocapnia in Ethiopian high altitude dwellers. Stroke 39, 336–342. https://doi.org/10.1161/STROKEAHA.107.491498.
Colley, B.S., Phillips, L.L., Reeves, T.M., 2010. The effects of cyclosporin-A on axonal conduction deficits following traumatic brain injury in adult rats. Exp. Neurol. 224, 241–251. https://doi.org/10.1016/j.expneurol.2010.03.026.
Coskren, P.J., Luebke, J.I., Kabaso, D., Wearne, S.L., Yadav, A., Rumbell, T., Hof, P.R., Weaver, C.M., 2015. Functional consequences of age-related morphologic changes to pyramidal neurons of the rhesus monkey prefrontal cortex. J. Comput. Neurosci. 38, 263–283. https://doi.org/10.1007/s10827-014-0541-5.
Cowell, S.A., Stocks, J.M., Evans, D.G., Simonson, S.R., Greenleaf, J.E., 2002. The exercise and environmental physiology of extravehicular activity. Aviat. Space Environ. Med. 73, 54–67.
Cramer, N.P., Xu, X., Christensen, C., Bierman, A., Tankersley, C.G., Galdzicki, Z., 2015. Strain variation in the adaptation of C57Bl6 and BALBc mice to chronic hypobaric hypoxia. Physiol. Behav. 143, 158–165. https://doi.org/10.1016/j.physbeh.2015.01.036.
De Peuter, S., Van Diest, I., Lemaigre, V., Verleden, G., Demedts, M., Van den Bergh, O., 2004. Dyspnea: the role of psychological processes. Clin. Psychol. Rev. 24, 557–581. https://doi.org/10.1016/j.cpr.2004.05.001.
Deshmukh, V.A., Tardif, V., Lyssiotis, C.A., Green, C.C., Kerman, B., Kim, H.J., Padmanabhan, K., Swoboda, J.G., Ahmad, I., Kondo, T., Gage, F.H., Theofilopoulos, A.N., Lawson, B.R., Schultz, P.G., Lairson, L.L., 2013. A regenerative approach to the treatment of multiple sclerosis. Nature 502, 327–332. https://doi.org/10.1038/nature12647.
Di Paola, M., Paola, M.D., Bozzali, M., Fadda, L., Musicco, M., Sabatini, U., Caltagirone, C., 2008. Reduced oxygen due to high-altitude exposure relates to atrophy in motor-function brain areas. Eur. J. Neurol. 15, 1050–1057. https://doi.org/10.1111/j.1468-1331.2008.02243.x.
Eid, T., Tu, N., Lee, T.-S.W., Lai, J.C.K., 2013. Regulation of astrocyte glutamine synthetase in epilepsy. Neurochem. Int. 63, 670–681. https://doi.org/10.1016/j.neuint.2013.06.008.
Fan, J.-L., Kayser, B., 2016. Fatigue and exhaustion in hypoxia: the role of cerebral oxygenation. High Alt. Med. Biol. 17, 72–84. https://doi.org/10.1089/ham.2016.0034.
Fayed, N., Modrego, P.J., Morales, H., 2006. Evidence of brain damage after high-altitude climbing by means of magnetic resonance imaging. Am. J. Med. 119. https://doi.org/10.1016/j.amjmed.2005.07.062.
Feddersen, B., Neupane, P., Thanbichler, F., Hadolt, I., Sattelmeyer, V., Pfefferkorn, T., Waanders, R., Noachtar, S., Ausserer, H., 2015. Regional differences in the cerebral blood flow velocity response to hypobaric hypoxia at high altitudes. J. Cereb. Blood Flow Metab. 35, 1846–1851. https://doi.org/10.1038/jcbfm.2015.142.
Foster, G.E., Davies-Thompson, J., Dominelli, P.B., Heran, M.K.S., Donnelly, J., Dumanoir, G.R., Ainslie, P.N., Rauscher, A., Sheel, A.W., 2015. Changes in cerebral vascular reactivity and structure following prolonged exposure to high altitude in humans. Physiol. Rep. 3, e12647. https://doi.org/10.14814/phy2.12647.
Fujioka, R., Nii, T., Iwaki, A., Shibata, A., Ito, I., Kitaichi, K., Nomura, M., Hattori, S., Takao, K., Miyakawa, T., Fukumaki, Y., 2014. Comprehensive behavioral study of mGluR3 knockout mice: implication in schizophrenia related endophenotypes. Mol. Brain 7, 31. https://doi.org/10.1186/1756-6606-7-31.
Garcia, J.A., Cardona, S.M., Cardona, A.E., 2013. Analyses of microglia effector function using CX3CR1-GFP knock-in mice. Methods Mol. Biol. 1041, 307–317. https://doi.org/10.1007/978-1-62703-520-0_27.
Gyorgy, B., Toth, E., Tarcsa, E., Falus, A., Buzas, E.I., 2006. Citrullination: a post-translational modification in health and disease. Int. J. Biochem. Cell Biol. 38, 1662–1677. https://doi.org/10.1016/j.biocel.2006.03.008.
Hackett, P.H., Yarnell, P.R., Hill, R., Reynard, K., Heit, J., McCormick, J., 1998. High-altitude cerebral edema evaluated with magnetic resonance imaging. JAMA 280, 1920. https://doi.org/10.1001/jama.280.22.1920.
Hagiwara, T., Tanaka, K., Takai, S., Maeno-Hikichi, Y., Mukainaka, Y., Wada, K., 1996. Genomic organization, promoter analysis, and chromosomal localization of the gene for the mouse glial high-affinity glutamate transporter Slc1a3. Genomics 33, 508–515. https://doi.org/10.1006/geno.1996.0226.
Hama, H., Kurokawa, H., Kawano, H., Ando, R., Shimogori, T., Noda, H., Fukami, K., Sakaue-Sawano, A., Miyawaki, A., 2011. Scale: a chemical approach for fluorescence imaging and reconstruction of transparent mouse brain. Nat. Neurosci. 14, 1481–1488. https://doi.org/10.1038/nn.2928.
Harashima, C., Jacobowitz, D.M., Stoffel, M., Chakrabarti, L., Haydar, T.F., Siarey, R.J., Galdzicki, Z., 2006a. Elevated expression of the G-protein-activated inwardly rectifying potassium channel 2 (GIRK2) in cerebellar unipolar brush cells of a Down syndrome mouse model. Cell. Mol. Neurobiol. 26, 719–734. https://doi.org/10.1007/s10571-006-9066-4.
Harashima, C., Jacobowitz, D.M., Witta, J., Borke, R.C., Best, T.K., Siarey, R.J., Galdzicki, Z., 2006b. Abnormal expression of the G-protein-activated inwardly rectifying potassium channel 2 (GIRK2) in hippocampus, frontal cortex, and substantia nigra of Ts65Dn mouse: a model of Down syndrome. J. Comp. Neurol. 494, 815–833. https://doi.org/10.1002/cne.20844.
Huang, J., Li, Y., Tang, Y., Tang, G., Yang, G.-Y., Wang, Y., 2013. CXCR4 antagonist AMD3100 protects blood-brain barrier integrity and reduces inflammatory response after focal ischemia in mice. Stroke 44, 190–197. https://doi.org/10.1161/STROKEAHA.112.670299.
Hunt, J.S., Theilmann, R.J., Smith, Z.M., Scadeng, M., Dubowitz, D.J., 2013. Cerebral diffusion and T(2): MRI predictors of acute mountain sickness during sustained high-altitude hypoxia. J. Cereb. Blood Flow Metab. 33, 372–380. https://doi.org/10.1038/jcbfm.2012.184.
Imray, C., Chan, C., Stubbings, A., Rhodes, H., Patey, S., Wilson, M.H., Bailey, D.M., Wright, A.D., Birmingham Medical Research Expeditionary Society, 2014. Time course variations in the mechanisms by which cerebral oxygen delivery is maintained on exposure to hypoxia/altitude. High Alt. Med. Biol. 15, 21–27. https://doi.org/10.1089/ham.2013.1079.
Jansen, G.F., Krins, A., Basnyat, B., Bosch, A., Odoom, J.A., 2000. Cerebral autoregulation in subjects adapted and not adapted to high altitude. Stroke 31, 2314–2318.
Kallenberg, K., Dehnert, C., Dörfler, A., Schellinger, P.D., Bailey, D.M., Knauth, M., Bärtsch, P.D., 2008. Microhemorrhages in nonfatal high-altitude cerebral edema. J. Cereb. Blood Flow Metab. 28, 1635–1642. https://doi.org/10.1038/jcbfm.2008.55.
Kauser, H., Sahu, S., Kumar, S., Panjwani, U., 2014. Guanfacine ameliorates hypobaric hypoxia induced spatial working memory deficits. Physiol. Behav. 123, 187–192. https://doi.org/10.1016/j.physbeh.2013.10.028.
Kneussel, M., Wagner, W., 2013. Myosin motors at neuronal synapses: drivers of membrane transport and actin dynamics. Nat. Rev. Neurosci. 14, 233–247. https://doi.org/10.1038/nrn3445.
Kottke, R., Pichler Hefti, J., Rummel, C., Hauf, M., Hefti, U., Merz, T.M., 2015. Morphological brain changes after climbing to extreme altitudes—a prospective cohort study. PLoS One 10, e0141097. https://doi.org/10.1371/journal.pone.0141097.
Kubo, K., Hanaoka, M., Hayano, T., Miyahara, T., Hachiya, T., Hayasaka, M., Koizumi, T., Fujimoto, K., Kobayashi, T., Honda, T., 1998. Inflammatory cytokines in BAL fluid and pulmonary hemodynamics in high-altitude pulmonary edema. Respir. Physiol. 111, 301–310.
Leaf, D.E., Goldfarb, D.S., 2007. Mechanisms of action of acetazolamide in the prophylaxis and treatment of acute mountain sickness. J. Appl. Physiol. 102, 1313–1322. https://doi.org/10.1152/japplphysiol.01572.2005.
Lemos, V. de A., dos Santos, R.V.T., Lira, F.S., Rodrigues, B., Tufik, S., de Mello, M.T., 2013. Can high altitude influence cytokines and sleep? Mediat. Inflamm. 2013, 279365. https://doi.org/10.1155/2013/279365.
León-Velarde, F., Maggiorini, M., Reeves, J.T., Aldashev, A., Asmus, I., Bernardi, L., Ge, R.-L., Hackett, P., Kobayashi, T., Moore, L.G., Penaloza, D., Richalet, J.-P., Roach, R., Wu, T., Vargas, E., Zubieta-Castillo, G., Zubieta-Calleja, G., 2005. Consensus statement on chronic and subacute high altitude diseases. High Alt. Med. Biol. 6, 147–157. https://doi.org/10.1089/ham.2005.6.147.
Love, M.I., Huber, W., Anders, S., 2014. Moderated estimation of fold change and dispersion for RNA-seq data with DESeq2. Genome Biol. 15, 550. https://doi.org/10.1186/PREACCEPT-8897612761307401.
Maiti, P., Singh, S.B., Mallick, B., Muthuraju, S., Ilavazhagan, G., 2008. High altitude memory impairment is due to neuronal apoptosis in hippocampus, cortex and striatum. J. Chem. Neuroanat. 36, 227–238. https://doi.org/10.1016/j.jchemneu.2008.07.003.
Man, S., Tucky, B., Cotleur, A., Drazba, J., Takeshita, Y., Ransohoff, R.M., 2012. CXCL12-induced monocyte-endothelial interactions promote lymphocyte transmigration across an in vitro blood-brain barrier. Sci. Transl. Med. 4, 119ra14. https://doi.org/10.1126/scitranslmed.3003197.
Mangiardi, M., Crawford, D.K., Xia, X., Du, S., Simon-Freeman, R., Voskuhl, R.R., Tiwari-Woodruff, S.K., 2011. An animal model of cortical and callosal pathology in multiple sclerosis. Brain Pathol. 21, 263–278. https://doi.org/10.1111/j.1750-3639.2010.00444.x.
Mathew, J.G., Basehore, S., Clyne, A.M., 2017. Fluid shear stress and fibroblast growth factor-2 increase endothelial cell-associated vitronectin. Appl. Bionics Biomech. 2017, 9040161. https://doi.org/10.1155/2017/9040161.
McCandless, E.E., Budde, M., Lees, J.R., Dorsey, D., Lyng, E., Klein, R.S., 2009. IL-1R

signaling within the central nervous system regulates CXCL12 expression at the blood-brain barrier and disease severity during experimental autoimmune encephalomyelitis. J. Immunol. 183, 613–620. https://doi.org/10.4049/jimmunol.0802258.
McGuire, S., Sherman, P., Profenna, L., Grogan, P., Sladky, J., Brown, A., Robinson, A., Rowland, L., Hong, E., Patel, B., Tate, D., Kawano, E.S., Fox, P., Kochunov, P., 2013. White matter hyperintensities on MRI in high-altitude U-2 pilots. Neurology 81, 729–735. https://doi.org/10.1212/WNL.0b013e3182a1ab12.
McGuire, S. a, Tate, D.F., Wood, J., Sladky, J.H., McDonald, K., Sherman, P.M., Kawano, E.S., Rowland, L.M., Patel, B., Wright, S.N., Hong, E., Rasmussen, J., Willis, A.M., Kochunov, P.V., 2014. Lower neurocognitive function in U-2 pilots: Relationship to white matter hyperintensities. Neurology 83, 1–8. https://doi.org/10.1212/WNL.0000000000000694.
Nayak, B.K., Shanmugasundaram, K., Friedrichs, W.E., Cavaglierii, R.C., Patel, M., Barnes, J., Block, K., 2016. HIF-1 mediates renal fibrosis in OVE26 type 1 diabetic mice. Diabetes 65, 1387–1397. https://doi.org/10.2337/db15-0519.
Nelson, T.O., Dunlosky, J., White, D.M., Steinberg, J., Townes, B.D., Anderson, D., 1990. Cognition and metacognition at extreme altitudes on Mount Everest. J. Exp. Psychol. Gen. 119, 367–374.
Netzer, N., Strohl, K., Faulhaber, M., Gatterer, H., Burtscher, M., 2013. Hypoxia-related altitude illnesses. J. Travel Med. 20, 247–255. https://doi.org/10.1111/jtm.12017.
Norcliffe, L.J., Rivera-Ch, M., Claydon, V.E., Moore, J.P., Leon-Velarde, F., Appenzeller, O., Hainsworth, R., 2005. Cerebrovascular responses to hypoxia and hypocapnia in high-altitude dwellers. J. Physiol. 566, 287–294. https://doi.org/10.1113/jphysiol.2005.086629.
Ohkawa, N., Kokura, K., Matsu-Ura, T., Obinata, T., Konishi, Y., Tamura, T.A., 2001. Molecular cloning and characterization of neural activity-related RING finger protein (NARF): A new member of the RBCC family is a candidate for the partner of myosin V. J. Neurochem. 78, 75–87. https://doi.org/10.1046/j.1471-4159.2001.00373.x.
Olmos-Serrano, J.L., Kang, H.J., Tyler, W.A., Silbereis, J.C., Cheng, F., Zhu, Y., Pletikos, M., Jankovic-Rapan, L., Cramer, N.P., Galdzicki, Z., Goodliffe, J., Peters, A., Sethares, C., Delalle, I., Golden, J.A., Haydar, T.F., Sestan, N., 2016. Down syndrome developmental brain transcriptome reveals defective oligodendrocyte differentiation and myelination. Neuron 89, 1208–1222. https://doi.org/10.1016/j.neuron.2016.01.042.
Prasad, J., Baitharu, I., Sharma, A.K., Dutta, R., Prasad, D., Singh, S.B., 2013. Quercetin reverses hypobaric hypoxia-induced hippocampal neurodegeneration and improves memory function in the rat. High Alt. Med. Biol. 14, 383–394. https://doi.org/10.1089/ham.2013.1014.
Real, C., Remedio, L., Caiado, F., Igreja, C., Borges, C., Trindade, A., Pinto-Do-O, P., Yagita, H., Duarte, A., Dias, S., 2011. Bone marrow-derived endothelial progenitors expressing Delta-like 4 (Dll4) regulate tumor angiogenesis. PLoS One 6, e18323. https://doi.org/10.1371/journal.pone.0018323.
Regard, M., Oelz, O., Brugger, P., Landis, T., 1989. Persistent cognitive impairment in climbers after repeated exposure to extreme altitude. Neurology 39, 210–213.
Richardson, C., Hogan, A.M., Bucks, R.S., Baya, A., Virues-Ortega, J., Holloway, J.W., Rose-Zerilli, M., Palmer, L.J., Webster, R.J., Kirkham, F.J., Baldeweg, T., 2011. Neurophysiological evidence for cognitive and brain functional adaptation in adolescents living at high altitude. Clin. Neurophysiol. 122, 1726–1734. https://doi.org/10.1016/j.clinph.2011.02.001.
Rimoldi, S.F., Rexhaj, E., Duplain, H., Urben, S., Billieux, J., Allemann, Y., Romero, C., Ayaviri, A., Salinas, C., Villena, M., Scherrer, U., Sartori, C., 2016. Acute and chronic altitude-induced cognitive dysfunction in children and adolescents. J. Pediatr. 169, 238–243. https://doi.org/10.1016/j.jpeds.2015.10.009.
Robertson, R.T., Levine, S.T., Haynes, S.M., Gutierrez, P., Baratta, J.L., Tan, Z., Longmuir, K.J., 2014. Use of labeled tomato lectin for imaging vasculature structures. Histochem. Cell Biol. 143, 225–234. https://doi.org/10.1007/s00418-014-1301-3.
Robinson, M.D., McCarthy, D.J., Smyth, G.K., 2010. edgeR: a bioconductor package for differential expression analysis of digital gene expression data. Bioinformatics 26, 139–140. https://doi.org/10.1093/bioinformatics/btp616.
Rumpel, H., Buchli, R., Gehrmann, J., Aguzzi, A., Illi, O., Martin, E., 1995. Magnetic resonance imaging of brain edema in the neonatal rat: a comparison of short and long term hypoxia-ischemia. Pediatr. Res. 38, 113–118. https://doi.org/10.1203/00006450-199507000-00020.
Ryn, Z., 1979. Nervous system and altitude syndrome of high altitude asthenia [WWW Document]. Acta Med. Pol. 20 (2), 155–169. http://eurekamag.com/research/005/965/005965427.php, Accessed date: 25 May 2016.
Ryn, Z., 1988. Psychopathology in mountaineering–mental disturbances under high-altitude stress. Int. J. Sports Med. 9, 163–169. https://doi.org/10.1055/s-2007-1024998.
Saunders, N.R., Dziegielewska, K.M., Møllgård, K., Habgood, M.D., 2015. Markers for blood-brain barrier integrity: how appropriate is Evans blue in the twenty-first century and what are the alternatives? Front. Neurosci. https://doi.org/10.3389/fnins.2015.00385.
Schmidt, M.V., Schulke, J.-P., Liebl, C., Stiess, M., Avrabos, C., Bock, J., Wochnik, G.M., Davies, H.A., Zimmermann, N., Scharf, S.H., Trumbach, D., Wurst, W., Zieglgansberger, W., Turck, C., Holsboer, F., Stewart, M.G., Bradke, F., Eder, M., Muller, M.B., Rein, T., 2011. Tumor suppressor down-regulated in renal cell carcinoma 1 (DRR1) is a stress-induced actin bundling factor that modulates synaptic efficacy and cognition. Proc. Natl. Acad. Sci. U. S. A. 108, 17213–17218. https://doi.org/10.1073/pnas.1103318108.
Schommer, K., Kallenberg, K., Lutz, K., Bärtsch, P., Knauth, M., 2013. Hemosiderin deposition in the brain as footprint of high-altitude cerebral edema. Neurology 81, 1776–1779. https://doi.org/10.1212/01.wnl.0000435563.84986.78.
Selvaraj, U.M., Ortega, S.B., Hu, R., Gilchrist, R., Kong, X., Partin, A., Plautz, E.J., Klein, R.S., Gidday, J.M., Stowe, A.M., 2017. Preconditioning-induced CXCL12 upregulation minimizes leukocyte infiltration after stroke in ischemia-tolerant mice. J. Cereb. Blood Flow Metab. 37, 801–813. https://doi.org/10.1177/0271678X16639327.
Semple, B.D., Blomgren, K., Gimlin, K., Ferriero, D.M., Noble-Haeusslein, L.J., 2013. Brain development in rodents and humans: Identifying benchmarks of maturation and vulnerability to injury across species. Prog. Neurobiol. 106–107, 1–16. https://doi.org/10.1016/j.pneurobio.2013.04.001.
Sharma, V.K., Das, S.K., Dhar, P., Hota, K.B., Mahapatra, B.B., Vashishtha, V., Kumar, A., Hota, S.K., Norboo, T., Srivastava, R.B., 2014. Domain specific changes in cognition at high altitude and its correlation with hyperhomocysteinemia. PLoS One 9, e101448. https://doi.org/10.1371/journal.pone.0101448.
Shukitt-Hale, B., Stillman, M.J., Welch, D.I., Levy, A., Devine, J.A., Lieberman, H.R., 1994. Hypobaric hypoxia impairs spatial memory in an elevation-dependent fashion. Behav. Neural Biol. 62, 244–252.
Smith, A., 2005. Hypoxia symptoms reported during helicopter operations below 10,000 ft: a retrospective survey. Aviat. Space Environ. Med. 76, 794–798.
Song, S.-K., Sun, S.-W., Ramsbottom, M.J., Chang, C., Russell, J., Cross, A.H., 2002. Dysmyelination revealed through MRI as increased radial (but unchanged axial) diffusion of water. NeuroImage 17, 1429–1436.
Stowe, A.M., Altay, T., Freie, A.B., Gidday, J.M., 2011. Repetitive hypoxia extends endogenous neurovascular protection for stroke. Ann. Neurol. 69, 975–985. https://doi.org/10.1002/ana.22367.
Subudhi, A.W., Bourdillon, N., Bucher, J., Davis, C., Elliott, J.E., Eutermoster, M., Evero, O., Fan, J.-L., Jameson-Van Houten, S., Julian, C.G., Kark, J., Kark, S., Kayser, B., Kern, J.P., Kim, S.E., Lathan, C., Laurie, S.S., Lovering, A.T., Paterson, R., Polaner, D.M., Ryan, B.J., Spira, J.L., Tsao, J.W., Wachsmuth, N.B., Roach, R.C., 2014. AltitudeOmics: the integrative physiology of human acclimatization to hypobaric hypoxia and its retention upon reascent. PLoS One 9, e92191. https://doi.org/10.1371/journal.pone.0092191.
Suidan, G.L., Brill, A., De Meyer, S.F., Voorhees, J.R., Cifuni, S.M., Cabral, J.E., Wagner, D.D., 2013. Endothelial Von Willebrand factor promotes blood-brain barrier flexibility and provides protection from hypoxia and seizures in mice. Arterioscler. Thromb. Vasc. Biol. 33, 2112–2120. https://doi.org/10.1161/ATVBAHA.113.301362.
Swenson, E.R., 2016. Pharmacology of acute mountain sickness: old drugs and newer thinking. J. Appl. Physiol. 120, 204–215. https://doi.org/10.1152/japplphysiol.00443.2015.
Tischner, D., Weishaupt, A., Van Den Brandt, J., Müller, N., Beyersdorf, N., Ip, C.W., Toyka, K.V., Hünig, T., Gold, R., Kerkau, T., Reichardt, H.M., 2006. Polyclonal expansion of regulatory T cells interferes with effector cell migration in a model of multiple sclerosis. Brain 129, 2635–2647. https://doi.org/10.1093/brain/awl213.
Titus, A.D.J., Shankaranarayana Rao, B.S., Harsha, H.N., Ramkumar, K., Srikumar, B.N., Singh, S.B., Chattarji, S., Raju, T.R., 2007. Hypobaric hypoxia-induced dendritic atrophy of hippocampal neurons is associated with cognitive impairment in adult rats. Neuroscience 145, 265–278. https://doi.org/10.1016/j.neuroscience.2006.11.037.
Virués-Ortega, J., Buela-Casal, G., Garrido, E., Alcázar, B., 2004. Neuropsychological functioning associated with high-altitude exposure. Neuropsychol. Rev. 14, 197–224.
Waligora, J.M., Horrigan, D.J., Nicogossian, A., 1991. The physiology of spacecraft and space suit atmosphere selection. Acta Astronaut. 23, 171–177.
Wang, S., Wu, E.X., Cai, K., Lau, H.-F., Cheung, P.-T., Khong, P.-L., 2009. Mild hypoxic-ischemic injury in the neonatal rat brain: longitudinal evaluation of white matter using diffusion tensor MR imaging. AJNR Am. J. Neuroradiol. 30, 1907–1913. https://doi.org/10.3174/ajnr.A1697.
West, J.B., 2004. The physiologic basis of high-altitude diseases. Ann. Intern. Med. 141, 789–800.
Wilson, David IG, Langston, Rosamund F, Schlesiger, Magdalene, Wagner, Monica, Watanabe, Sakurako, Ainge, James A, 2013 May. Lateral Entorhinal Cortex is Critical for Novel Object-Context Recognition. Hippocampus 23 (5), 352–366.
Willie, C.K., MacLeod, D.B., Smith, K.J., Lewis, N.C., Foster, G.E., Ikeda, K., Hoiland, R.L., Ainslie, P.N., 2015. The contribution of arterial blood gases in cerebral blood flow regulation and fuel utilization in man at high altitude. J. Cereb. Blood Flow Metab. 35, 873–881. https://doi.org/10.1038/jcbfm.2015.4.
Yan, X., Zhang, J., Shi, J., Gong, Q., Weng, X., 2010. Cerebral and functional adaptation with chronic hypoxia exposure: a multi-modal MRI study. Brain Res. 1348, 21–29. https://doi.org/10.1016/j.brainres.2010.06.024.
Yan, X., Zhang, J., Gong, Q., Weng, X., 2011. Adaptive influence of long term high altitude residence on spatial working memory: an fMRI study. Brain Cogn. 77, 53–59. https://doi.org/10.1016/j.bandc.2011.06.002.
Zhang, H., Lin, J., Sun, Y., Huang, Y., Ye, H., Wang, X., Yang, T., Jiang, X., Zhang, J., 2012. Compromised white matter microstructural integrity after mountain climbing: evidence from diffusion tensor imaging. High Alt. Med. Biol. 13, 118–125. https://doi.org/10.1089/ham.2011.1073.
Zhang, G., Zhou, S.-M., Yuan, C., Tian, H.-J., Li, P., Gao, Y.-Q., 2013. The effects of short-term and long-term exposure to a high altitude hypoxic environment on neurobehavioral function. High Alt. Med. Biol. 14, 338–341. https://doi.org/10.1089/ham.2012.1091.
Zhao, F.-Q., Keating, A.F., 2007. Functional properties and genomics of glucose transporters. Curr. Genomics 8, 113–128.